



## ORIGINAL ARTICLE OPEN ACCESS

# Development of a Preclinical Double Model of Mandibular Irradiated Bone and Osteoradionecrosis in New Zealand Rabbits

Alessandra Ruaro<sup>1,2,3</sup> | Stefano Taboni<sup>1,2,3</sup>  | Harley H. L. Chan<sup>4</sup> | Tiziana Mondello<sup>2,3</sup> | Patricia Lindsay<sup>5</sup> | Teesha Komal<sup>6</sup> | Lara Alessandrini<sup>7</sup> | Marta Sbaraglia<sup>7</sup> | Elena Bellan<sup>7</sup> | Roberto Maroldi<sup>8</sup> | Jason Townson<sup>4</sup> | Michael J. Daly<sup>4</sup> | Federica Re<sup>9,10</sup> | Chiara Pasini<sup>11</sup> | Marco Krengli<sup>12,13</sup> | Luciana Sartore<sup>11</sup> | Domenico Russo<sup>9</sup> | Piero Nicolai<sup>2,3</sup> | Marco Ferrari<sup>1,2,3</sup>  | Ralph W. Gilbert<sup>14</sup> | Jonathan C. Irish<sup>4,14</sup>

<sup>1</sup>Guided Therapeutics (GTx) Program, International Scholarship Program, Techna Institute, University Health Network, Toronto, Ontario, Canada | <sup>2</sup>Section of Otorhinolaryngology—Head and Neck Surgery, Department of Neurosciences, University of Padova, Padova, Italy | <sup>3</sup>Unit of Otorhinolaryngology—Head and Neck Surgery, Azienda Ospedale Università di Padova, Padova, Italy | <sup>4</sup>Guided Therapeutics (GTx) Program, Princess Margaret Cancer Centre, Toronto, Ontario, Canada | <sup>5</sup>Department of Radiation Oncology, Radiation Physics, and Princess Margaret Hospital, University of Toronto, Toronto, Ontario, Canada | <sup>6</sup>Spatio-Temporal Targeting and Amplification of Radiation (STTARR) Innovation Centre, University Health Network, Toronto, Ontario, Canada | <sup>7</sup>Department of Medicine (DIMED), University of Padova, Padova, Italy | <sup>8</sup>Radiology Unit, ASST Spedali Civili di Brescia, University of Brescia, Brescia, Italy | <sup>9</sup>Unit of Blood Diseases and Bone Marrow Transplantation, Department of Clinical and Experimental Sciences, ASST Spedali Civili, University of Brescia, Brescia, Italy | <sup>10</sup>Centro di Ricerca Emato-Oncologica AIL (CREA), ASST Spedali Civili, Brescia, Italy | <sup>11</sup>Department of Mechanical and Industrial Engineering, University of Brescia, Brescia, Italy | <sup>12</sup>Radiotherapy Unit, Veneto Institute of Oncology IOV—IRCCS, Padova, Italy | <sup>13</sup>Department of Surgery, Oncology and Gastroenterology (DISCOG), University of Padova, Padova, Italy | <sup>14</sup>Princess Margaret Cancer Centre/Toronto General Hospital, Department of Otolaryngology-Head and Neck Surgery/Surgical Oncology, University Health Network, Toronto, Ontario, Canada

**Correspondence:** Jonathan C. Irish ([jonathan.irish@uhn.ca](mailto:jonathan.irish@uhn.ca))

**Received:** 2 July 2024 | **Revised:** 12 September 2024 | **Accepted:** 21 September 2024

**Section Editor:** Dennis H. Kraus

**Funding:** This work was supported by Princess Margaret Cancer Foundation.

**Keywords:** experimental animal models | head and neck | mandibular irradiation | osteoradionecrosis | radiotherapy

## ABSTRACT

**Purpose:** Radiotherapy (RT) plays a crucial role in head and neck (HN) cancer treatment. Nevertheless, it can lead to serious and challenging adverse events such as osteoradionecrosis (ORN). A preclinical rabbit model of irradiated bone and ORN is herein proposed, with the aim to develop a viable model to be exploited for investigating new therapeutic approaches.

**Methods:** Nine New Zealand white rabbits were irradiated using a single beam positioned to the left of the mandible and directed perpendicular to the left mandible. A  $10 \times 10 \text{ mm}^2$  region of interest (ROI) located below the first molar tooth on the left side was identified and irradiated with 7 Gy each fraction, once every 2 days, for five fractions. Dose distributions demonstrated that the corresponding ROI on the contralateral (right) mandibular side received approximately 5 Gy each fraction, thus bilateral irradiation of the mandible was achieved. ROIs were categorized as ROI<sub>H</sub> on the left side receiving the high dose and ROI<sub>L</sub> on the right side receiving the low dose. Rabbits were followed up clinically and imaged monthly. After 4 months, the irradiated bone was excised, and histological examination of ROIs was performed.

**Results:** Radiological signs suggestive for ORN were detected in the entire population (100%) 16 weeks after irradiation on ROI<sub>H</sub>, which consisted of cortical erosion and loss of trabeculae. ROI<sub>L</sub> did not show any radiological evidence of bone damage.

The last four authors equally share the last authorship.

This is an open access article under the terms of the [Creative Commons Attribution-NonCommercial-NoDerivs](https://creativecommons.org/licenses/by-nc-nd/4.0/) License, which permits use and distribution in any medium, provided the original work is properly cited, the use is non-commercial and no modifications or adaptations are made.

© 2024 The Author(s). *Head & Neck* published by Wiley Periodicals LLC.

Histologically, both sides showed comparable signs of injury, with marked reduction in osteocyte count and increase in empty lacunae count.

**Conclusions:** A preclinical double model was successfully developed. The side receiving the higher dose showed radiological and histological signs of bone damage, resulting in an ORN model. Whereas the contralateral side, receiving the lower dose, presented with histological damage only and a normal radiological appearance. This work describes the creation of a double model, an ORN and irradiated bone model, for further study using this animal species.

## 1 | Introduction

A multimodal treatment is often required in cancers of the head and neck (HN), including surgery, radiation therapy (RT), and/or chemotherapy.

RT plays a crucial role in HN malignancies both in the definitive and in adjuvant setting [1, 2]. However, RT poses many challenges due to the need for high-dose radiation in areas that are close to relevant organs at risk (i.e., brain tissue, orbit, and internal/common carotid artery) and/or structures involved in essential functions, strongly impacting a cancer survivor's quality of life [3].

The craniofacial skeleton can be affected by RT-related adverse events with different degrees of severity. RT-induced injury can manifest through dental implant failure [4], indirectly indicating the impact on underlying bone tissue; in other cases, damage can evolve to osteoradionecrosis (ORN), which represents one of the most significant complications following HN cancer treatment [5–7].

Despite its clinical importance, a universally accepted definition of ORN is still lacking [5, 8]. Historically, ORN has been defined as an area of exposed bone that does not heal spontaneously and persists for more than 3–6 months, without evidence of persistent or recurrent disease [9, 10]. Additionally, ORN pathogenesis remains controversial despite several mechanisms being hypothesized. Originally, bone necrosis seen in ORN was thought to be secondary to local trauma and its subsequent superinfection [11]. In 1983, Marx proposed RT-induced endarteritis as the *primum movens* leading to hypoxia, hypocellularity, and hypovascularity [10]. Twenty years later, Delanian and Lefaix proposed the “fibro-atrophic theory,” identifying as driving mechanisms the activation and dysregulation of fibroblasts [12]. With ORN pathogenesis still

debated, preclinical models would be useful to further explore the underlying biological mechanisms, and, consequently, to test different therapeutic approaches.

Although mandibular ORN incidence in patients treated for HN cancers has decreased over the years, current evidence suggests a prevalence of approximately 5%. Correlation between radionecrosis and total dose and dose per fraction is constantly reported, as well as the association with risk factors such as previous surgical procedure, concomitant chemotherapy, dental status, smoking history, alcohol consumption, and diabetes mellitus [13–15].

A multimodal approach is key for ORN management [16]. Treatments are variable, and options range from conservative approaches to surgical treatment, which could consist of simple debridement/curettage of the wound or more complex procedures such as free tissue transfer [17]. However, current available therapeutic strategies are debated and clinical evidence is weak [18].

In the present study, a preclinical animal model of (i) irradiated bone and (ii) ORN was developed to provide a reliable means to examine and test novel alternatives to manage ORN. Moreover, this model could be exploited to further explore the mechanisms that underlie pathogenesis of ORN.

## 2 | Methods and Materials

### 2.1 | Study Summary and Workflow

The study has been conducted in accordance with the international standard on animal welfare (National Institute of Health [NIH]) and has been approved by the University Health Network Animal Care Committee (Princess Margaret Cancer Centre, University Health Network, University of Toronto).

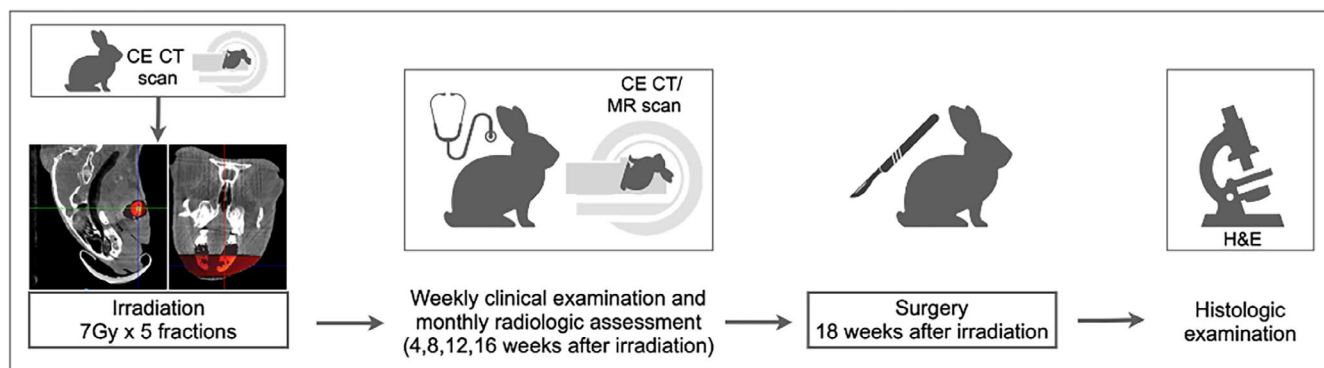


**FIGURE 1** | Study workflow. CE, contrast-enhanced; CT, computed tomography; MR, magnetic resonance; H&E, hematoxylin–eosin staining. [Color figure can be viewed at [wileyonlinelibrary.com](https://onlinelibrary.wiley.com)]

A high-level summary of the study is reported here, with full technical details presented in subsequent sections (Figure 1).

Nine New Zealand rabbits (*Oryctolagus cuniculus*) were included. First, a contrast-enhanced computed tomography scan (CECT) was performed. Then, the entire population was irradiated targeting the region of interest (ROI) of the mandible using a square collimator of  $10 \times 10 \text{ mm}^2$ . ROI was defined as a full-thickness,  $10 \times 10 \text{ mm}$  portion of the left mandibular body, located below the first molar root. A single beam was perpendicularly directed to ROI; the same dose has been prescribed in each rabbit: 7 Gy each fraction, once every 2 days, for a total of five fractions (35 Gy of total dose). Due to tissue attenuation, the contralateral mandibular body (right side) received a lower dose, estimated around 5 Gy per fraction. ROIs were categorized as ROI<sub>H</sub> on the side receiving the high dose (left side) and ROI<sub>L</sub> on the side receiving the low dose (right side).

All rabbits have been monitored clinically and radiologically to identify early signs of bone damage. The radiologic assessment was performed with CECT 4, 12, and 16 weeks after irradiation and with contrast-enhanced magnetic resonance (CE-MR) 8 weeks after irradiation. The scientific endpoint of the study (i.e., when surgery is indicated) was defined as the radiologic evidence of bone damage in at least 90% of the study sample.

Once the scientific endpoint was achieved, the entire population underwent survival surgery, which consisted of a bilateral inferior mandibulectomy centered in the irradiated target areas. Bone specimens were then examined histologically.

## 2.2 | Animal Model

The study was realized in immunocompetent male White New Zealand rabbits, *Oryctolagus cuniculus*, weighing 3 or more kg. The animals arrived at the Max Bell Research Centre (Toronto, Canada) at least a week before starting the project to allow acclimation.

## 2.3 | Irradiation Dose

Irradiation was performed with X-Rad 225 Cx Precision X-Ray, Inc. (North Brantford, CT, USA, voltage: 225 kVp, current: 13 mA) at the STTARR Innovation Centre (PMCRT, Toronto, Canada). In each rabbit, the mandibular target was irradiated with a total dose of 35 Gy in five fractions (7 Gy per fraction), delivered every 2 days. The beam-on times used for these experiments were based on doses calculated at 2 cm depth, without correction for tissue heterogeneity, and reported as dose-to-soft tissue (details in [Supporting Information](#)) [19, 20].

## 2.4 | Image-Guided Irradiation Planning and Development of a Double Model

Before irradiation, each rabbit underwent a cone-beam CT (scanning parameters: 60 kVp, 5 mA) on the X-Rad system to localize the target area, corresponding to the left mandibular

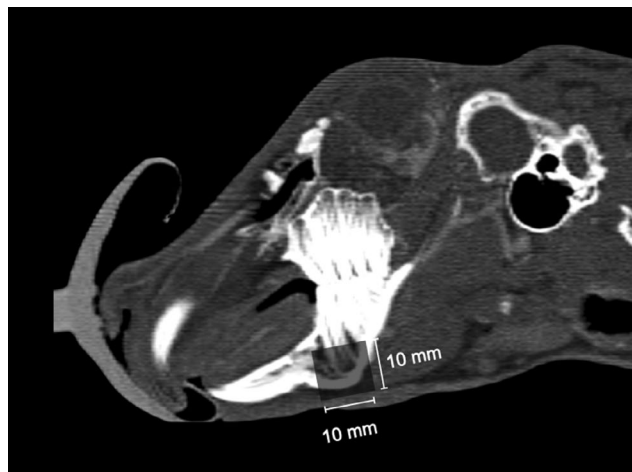


**FIGURE 2** | Irradiated target area. Bidimensional target localized at the inferior border of the mandible, below the root of the first molar (the irradiated area is marked in black).

body, caudally to the root of the first molar (Figure 2). The single beam source was positioned to the left side of the rabbit and directed transversally to the mandible; therefore, this setting enabled simultaneous bilateral mandible irradiation. In particular, ROI<sub>H</sub>, at the left mandibular body, has been irradiated with 7 Gy each fraction for a total dose of 35 Gy. ROI<sub>L</sub>, at the right hemimandible, received a dose corresponding to 65%–70% of the total dose (i.e., roughly 25 Gy, 5 Gy in each fraction) according to the dose distribution (Figure 3).

## 2.5 | Postirradiation Clinical and Radiologic Assessment

Once irradiation was completed, rabbits were carefully monitored clinically and radiologically with the aim of early identification of any clinical-radiologic sign of bone and/or soft tissue changes.

All rabbits underwent weekly examinations by veterinary clinicians and a HN surgeon to evaluate the intraoral soft tissues and the perimandibular skin included in the irradiation field. Radiologic examination (CT or MR, see below) was carried out under deep sedation maintained via 2.0%–2.5% isoflurane in 2 L/min oxygen.

CT scans (GE Revolution Frontier—Milwaukee, United States, voltage 100 kV, current: 750 mA, helical scanning [0.4 s] rotation,  $1024 \times 1024$  matrix, HD bone plus recon algorithm, slice thickness 0.625 mm, variable pixel spacing: 0.1–0.15 mm) with contrast enhancement (Omnipaque iodine contrast agent [GE Healthcare, Chicago, IL, USA]) were performed 4, 12, and 16 weeks after irradiation. The same scan was also performed prior to irradiation, to define the baseline radiologic characteristics of the irradiated areas.

MR (Siemens Healthineers, Erlangen, DE, 1.5 Tesla Aera system, with XJ gradient system,  $256 \times 256$  matrix over  $12 \times 12 \text{ cm}$  field-of-view for 0.5 mm in-plane resolution) with contrast enhancement (Gadovist, Bayer, Leverkusen, DE, dose of 0.3 mmol/kg)

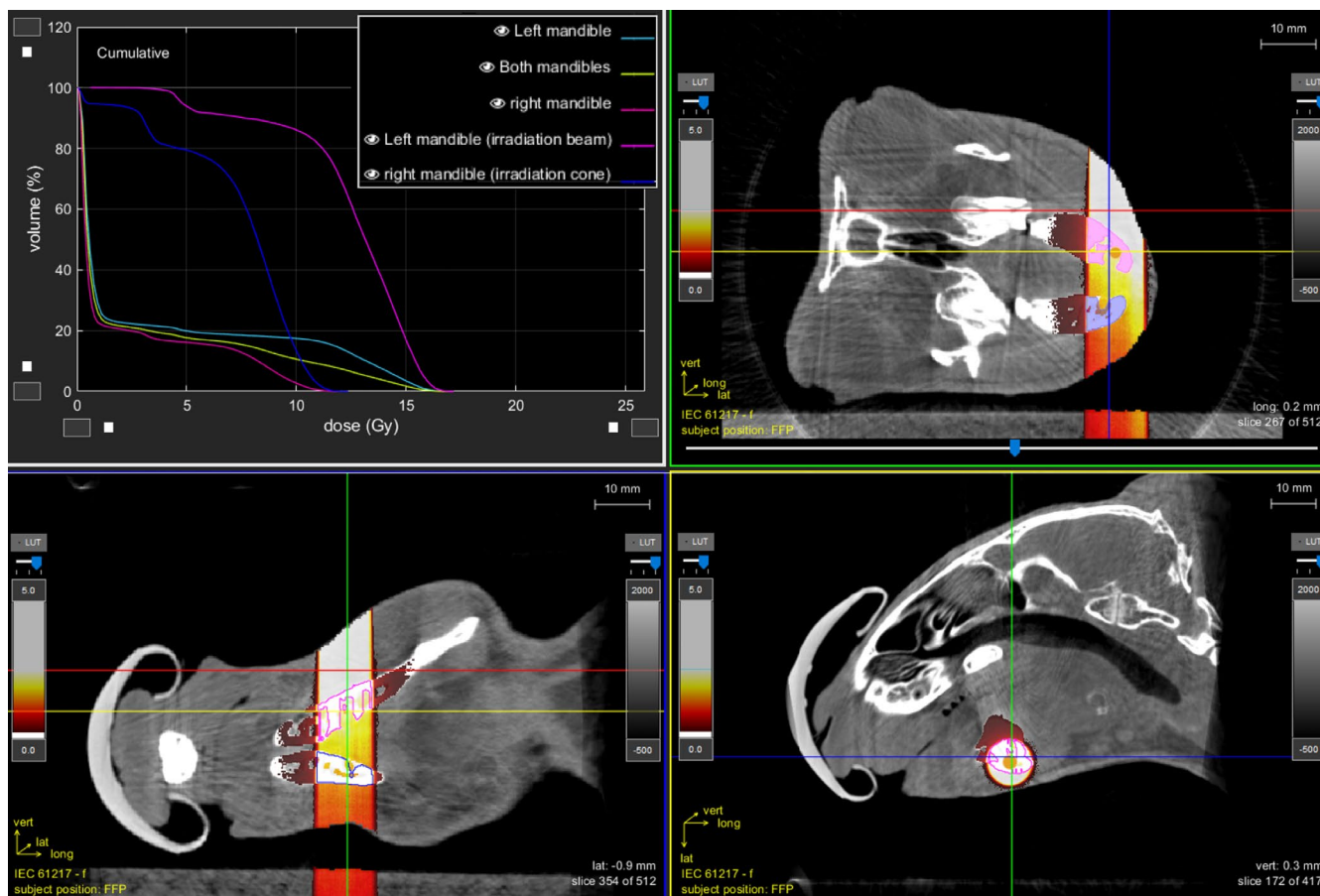


**FIGURE 3** | Dose distributions. The figure shows the irradiation dose distribution. The irradiation, sourced from the left of the animal, reached both the left and right mandibular bodies with decreasing dose. The dose distribution map revealed that the right mandibular body received approximately 5 Gy/fraction. [Color figure can be viewed at [wileyonlinelibrary.com](https://onlinelibrary.wiley.com)]

was acquired 8 weeks after irradiation, with 2D T2-weighted and 3D T1-weighted imaging protocol in the coronal plane.

The combination of the two scanning methods was selected to increase the probability of early detection of RT-induced changes in the bone and surrounding soft tissues.

## 2.6 | Radiologic Evaluation Criteria to Define Bone Damage

Images obtained with CT and MR were evaluated by an expert HN radiologist and two HN surgeons. The following parameters were considered suggestive for ORN at the CT scan: (1) uni- (i.e., related to either the lingual or the buccal cortical bone) or bi-cortical (i.e., related to both) bone erosion, (2) loss of trabeculae in the medullary bone, (3) bone sequestrum (i.e., a bone fragment totally separated from the adjacent bony areas). A radiologic score of ORN was obtained by summing the single scores assigned to the aforementioned parameters (Table S1). “Severe ORN” was arbitrarily defined by the presence of complete bicortical erosion and/or bone sequestrum [21].

MR images were evaluated to check for the following findings, which were considered as early signs of RT-induced

inflammation in the medullary bone [21]: (1) hypointensity in T1-weighted sequences, (2) hyperintensity in T2-weighted sequences, (3) marked enhancement in T1-weighted sequences after gadolinium administration.

## 2.7 | Analysis of Postirradiation Bone Density

The irradiated area was manually segmented (Mimics version 21.0, Materialize) in the pre-irradiation non-CECT scan and translated to each postirradiation non-CECT by means of co-registration, in order to ensure topographic consistency throughout measurements. Thus, the average density at the irradiated site was measured in each segmented area and relative density (RD) with respect to preoperative status was assessed (Supporting Information).

## 2.8 | Surgical Procedure

Surgery was performed 126–133 days after irradiation. All rabbits underwent a bilateral inferior marginal mandibulectomy under general anesthesia and laryngeal mask intubation. The inferior border of the mandible was exposed bilaterally through a 2 cm incision along the midline of the suprahyoid area.

Periosteum and muscular insertions were dissected off the inferior aspect of the mandibular body and removed. Defects of  $5 \times 5 \times 5 \text{ mm}^3$  were performed in the center of the irradiation area at the inferior border of the mandible by using a reciprocating saw (Figure S1 and Supporting Information).

## 2.9 | Histological Analysis of Irradiated Bone Tissue

The surgical specimen underwent decalcification with ethylenediaminetetraacetic acid (EDTA) and the completion was checked with radiography. Each sample was dehydrated and embedded in paraffin. Histological sections of  $4 \mu\text{m}$  were stained with hematoxylin and eosin (Bio-Optica) (StatLab, McKinney, TX) to analyze general tissue morphology.

The slides were digitized with Aperio AT2 brightfield scanner (Leica Biosystems, Concord, ON, Canada) and visualized with Aperio ImageScope 12.3.3 (Leica Biosystems Imaging Inc., Vista, Canada). Two different HN dedicated pathologists examined the specimen, considering the following parameters: (1) mean number of osteocytes/high-power field (HPF); (2) mean number of empty bony lacunae/HPF; (3) the presence of at least one of the following elements: (a) hyalinization and fibrosis with loss of bone marrow cells, (b) necrotic/sclerotic bone, (c) irregular bony trabeculae, (d) necrosis of the bone marrow with fibromyxoid tissue. As control, four additional specimens obtained from nonirradiated rabbit bone were processed and examined following the same protocol described above.

## 2.10 | Monitoring and Assessment of Adverse Events

For the entire length of the study, animals underwent regular clinical control, including evaluation of the overall status, weight, feeding capacity, signs of pain, urinary and fecal output, and body temperature.

Biochemical monitoring with complete blood count (CBC) and renal and liver function was performed monthly.

According to the animal use protocol, in case of severe adverse events the animal might reach the humane endpoint, prompting the need for euthanasia. Humane endpoints were defined in case of persistent abnormal posture, untreatable anorexia and dehydration, persistent self-trauma, hemorrhagic discharge, and surgical site alterations compromising normal behavior, or causing dysphagia.

## 2.11 | Statistical Analysis

Statistical analysis was performed using R Studio (Version 1.2.5042). Two types of data were gathered for analysis: (1) longitudinal data (time-to-endpoint data) and (2) endpoint data.

Longitudinal data included RD (quantitative variable) and the presence of radiological signs of bone damage (qualitative

variable), whereas the second group (i.e., endpoint data) included the histological bone characteristics. These data were considered as the response variables. The association of response variables with the total dose of irradiation (35 Gy vs. 25 Gy) was studied. Longitudinal quantitative data were modeled as nonlinear models and graphically rendered through generalized additive model-generated regression lines on scatter plots. Comparison between explanatory variable-determined subgroups was performed through analysis of variance with Tukey-adjusted post hoc test. The longitudinal qualitative data have been analyzed through cumulative incidence at the following time points: 4, 12, and 16 weeks after irradiation. Endpoint data have been graphically rendered through histogram and analyzed through the Mann-Whitney test. Significance was set at 0.05 for all statistical tests.

## 2.12 | Ethics

The latest amendment of the protocol (AUP#6010.6.2) was approved by the University Health Network Animal Care Committee (Princess Margaret Cancer Centre, University Health Network, University of Toronto) in July 2023. All the authors have confirmed their duty with respect to the rules defined by the ethics committee.

## 3 | Results

### 3.1 | Clinical Monitoring and Adverse Events

As the third fraction was administered, Three of the nine rabbits (33%) showed mild alopecia in the infrahyoid area. Sixteen weeks after irradiation, all rabbits presented with alopecia of various entity, without skin lesions or signs of superinfection. Three of the nine rabbits developed a 1 cm soft tissue swelling in the left perimandibular region, which spontaneously healed after a few weeks. Neither inflammatory lesions, ulcers, or bone exposure were observed in the oral cavity over the entire follow-up time. The entire population had an adequate oral feeding, and weight remained stable over the study period. No irradiation-related major adverse events were observed during the study period. One rabbit died during MR acquisition. The autptic examination did not clarify the cause of death but was compatible with acute respiratory failure (e.g., caused by laryngeal mask mispositioning).

### 3.2 | Radiologic Evidence of Bone Damage After Irradiation

Over the entire postirradiation period,  $\text{ROI}_L$  did not show radiologic signs of bone damage in any rabbit. On the contrary, signs of bone injury were observed in  $\text{ROI}_H$ . Two rabbits (25.0%) showed signs of bone alteration after 4 weeks (Figure 4), presenting unicortical erosion. After 12 weeks, 87.5% of rabbits presented cortical erosion (37.5% unicortical and 50.0% bicortical) and 62.5% showed loss of bone trabeculae. After 16 weeks, the entire population (100%) had cortical erosion (25.0% unicortical and 75.0% bicortical) and loss of trabeculae; 12.5% showed bone sequestrum. Considered altogether, signs suggestive for ORN were evident in 25.0% and 100% of rabbits after 4 and 16 weeks,

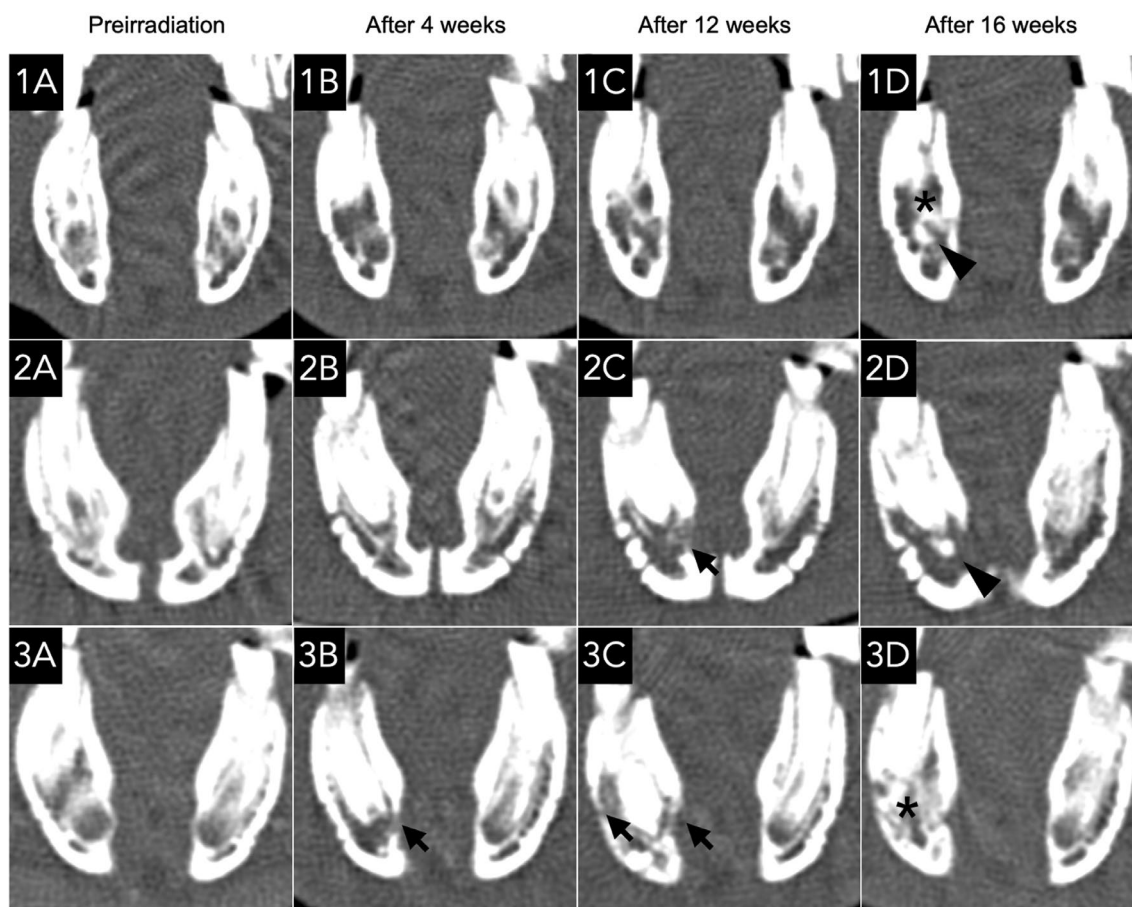


**FIGURE 4** | Radiologic signs of ORN on ROI<sub>H</sub> over the study period. Three explanatory examples of development of radiologic signs of bone injury at the different timepoints: Pre-RT (A), 4 weeks (B), 12 weeks (C), and 16 weeks (D) after irradiation. Coronal sections are displayed (in posteroanterior vision, left mandibular body correspond to the left of the image). Case 1: First signs of ORN consisted of loss of trabeculae (asterisk) and bone sclerosis (arrowhead) of the left mandible, detected 16 weeks after irradiation (1D). Case 2: First signs of ORN occurred 12 weeks after irradiation, with extended unicortical erosion on the lingual side of the left mandible (arrow) (2C); bone sequestrum was evident 16 weeks after irradiation (arrowhead) (2D). Case 3: Radiologic signs of bone damage were evident 4 weeks after irradiation (3B), with unicortical erosion on the lingual side (arrow) of the left mandible; bicortical erosion appeared 12 weeks after irradiation (arrows) (3C) and loss of trabeculae (asterisk) 16 weeks after the irradiation (3D).

**TABLE 1** | Specific outcomes in terms of radiologic signs of osteoradionecrosis (ORN) on the ROI<sub>H</sub> over the study period.

Outcome	Rate after 4 weeks (%)	Rate after 12 weeks (%)	Preoperative rate (after 16 weeks) (%)
Ipsilateral (total dose: 35/5 Gy)			
Unicortical erosion CI	25.0	87.5	100
Bicortical erosion CI	0.0	50.0	75.0
Bone sequestrum CI	0.0	0.0	12.5
Loss of trabeculae CI	0.0	62.5	100
CI of any sign of ORN	25.0	87.5	100
CI of severe ORN	0.0	50.0	75.0

Abbreviation: CI, cumulative incidence.

respectively. Radiologic signs of severe ORN were described in 50.0% and 100% of the population after 12 and 16 weeks, respectively (Table 1 and Figure 4).

On MR, a mild thickening and enhancement of mandibular periosteum in proximity of ROI<sub>H</sub> was detected in three (37.5%) rabbits after 8 weeks (Figure S2).

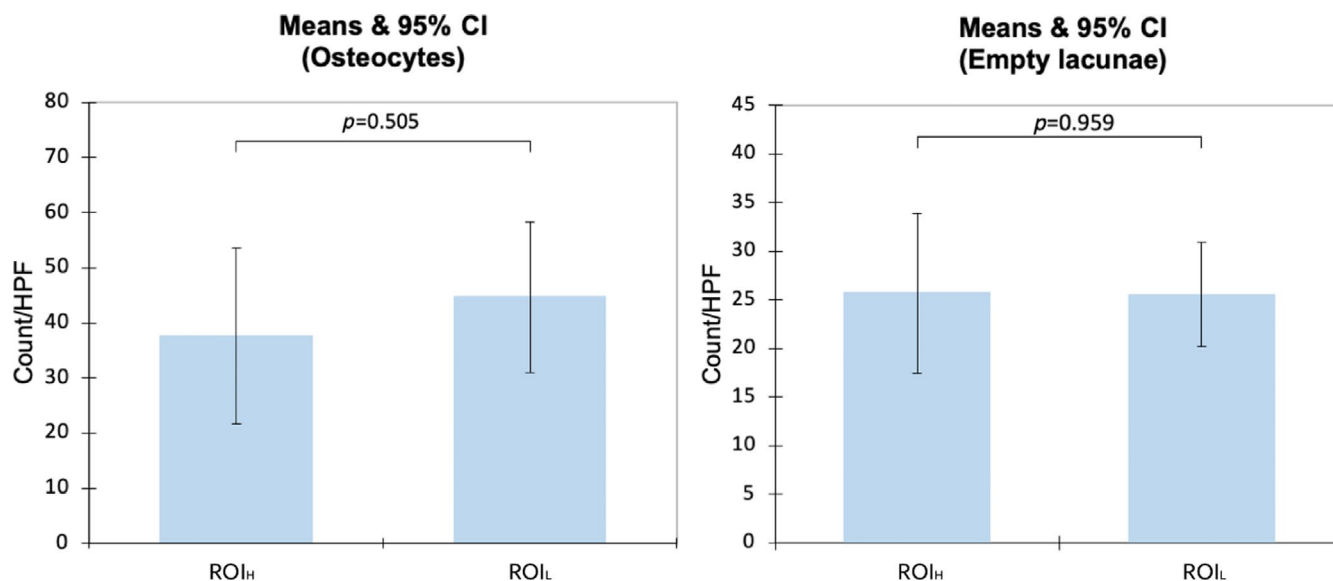


**FIGURE 5** | Osteocytes and empty lacunae count. Description through histograms of the mean and 95% confidence interval (95% CI) of osteocytes (left) and empty lacunae (right) count in irradiated bone. No statistical differences were observed in terms of osteocytes and empty lacunae count between the high-dose (35 Gy) and low-dose (25 Gy) groups. ROI<sub>H</sub> = region of interest irradiated with high dose; ROI<sub>L</sub> = region of interest irradiated with low dose. [Color figure can be viewed at [wileyonlinelibrary.com](https://onlinelibrary.wiley.com)]

### 3.3 | Histologic Evidence of Bone Damage After Irradiation

The mean count/HPF of osteocytes in ROI<sub>L</sub> and ROI<sub>H</sub> was 44.7 and 37.6, respectively. The mean count/HPF of empty bony lacunae was 25.5 versus 25.7, respectively. None of these differences was statistically significant (Figure 5). In addition, other parameters associated with microscopic bone injury (details in paragraph 2.9) were pronouncedly visible in all the specimens examined bilaterally (Figure 6). The mean count/HPF of osteocytes and empty lacunae in nonirradiated bone resulted 82.1 and 14.5, respectively.

### 3.4 | In Vivo Analysis of Bone Density of Irradiated Bone

The RD trend observed over the postirradiation phase did not show significant modification (Figure S3). No significant differences were observed when comparing ROI<sub>L</sub> with ROI<sub>H</sub> ( $p=0.120$ ).

## 4 | Discussion

RT can lead to a variety of tissue changes, with ORN representing one of the most challenging complications. ORN can present with different degrees of severity, ranging from clinically asymptomatic conditions to highly critical scenarios [5–7]. Also, RT can induce a subclinical bone injury resulting in dental decay and loss and dental implant [22].

As the dose distribution showed (Figure 3), the RT setting used in this study enabled bilateral mandibular irradiation, allowing to simultaneously test two different doses, namely 7 and 5 Gy per fraction, received by the mandibular body ipsilateral (left side)

and contralateral (right side) to the beam source, respectively. Here, ROI was centered on the molar region to develop models with a focus on areas most frequently affected by mandibular ORN in humans, including the premolar, molar, and retromolar areas of the mandible [23].

In vivo CT was employed to check for typical signs of ORN [21]. On ROI<sub>H</sub>, the entire cohort presented evidence of ORN after 16 weeks, with 75% of rabbits displaying severe ORN. Whereas on ROI<sub>L</sub>, no radiologic signs of bone damage were detected over the entire follow-up period. Hence, these data suggested that when five fractions are delivered, the dose of 7 Gy per fraction induces a radiologically evident bone damage, whereas 5 Gy per fraction is insufficient to generate a radiologically detectable bone injury.

CT scans were also performed to measure bone RD of ROI over time. Nevertheless, the RD trend did not show any significant variation both on ROI<sub>H</sub> and ROI<sub>L</sub>. We concluded that this methodology, which our group has previously successfully used to evaluate bone density variations in a bone regenerative setting [24], was inadequate in detecting underlying bone alterations in the present model. The hypothesis is that, in addition to the demineralization phenomena (i.e., cortical erosion and loss of trabeculae), other RT-induced bone alterations (i.e., bone sclerosis) can increase the CT density of the irradiated area [25, 26] (Figure 4). Thus, it is reasonable to assume that concurrence of these two competitive phenomena resulted in a flat trend of RD.

Universally approved criteria for histologic definition of ORN is still lacking. Nevertheless, reduced number of osteocytes, increased count in empty lacunae, as well as hyalinization, fibrosis/sclerosis, edema of the bone marrow, and necrosis are recognized as ORN-related features [27, 28]. In ours and other studies, substantial reduction of osteocytes and significant

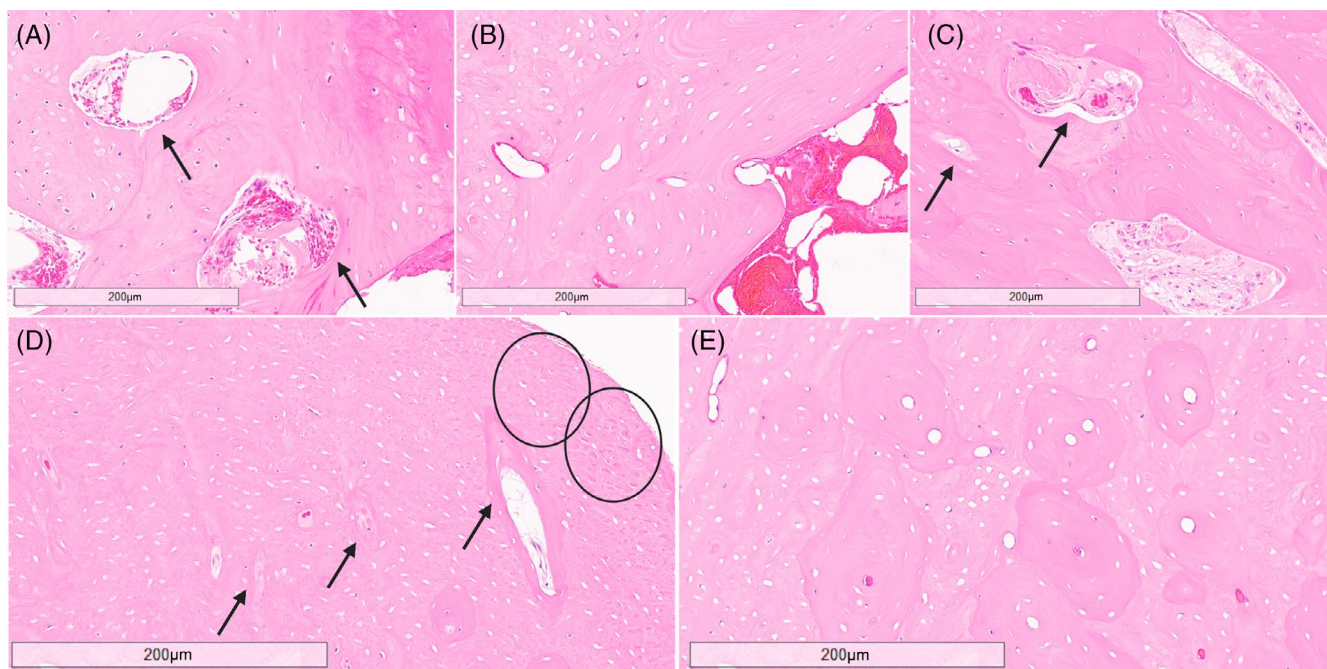


**FIGURE 6** | Histological signs of postirradiation bone damage. (A) Histological section that shows bone marrow damage with initial loss of hematopoietic cells (arrows). (B) Example of hemorrhagic bone marrow surrounded by empty lacunae. (C) Bone marrow with initial signs of vessel hyalinization and loss of cellularity (arrows). (D) Diffuse damage of the bone matrix: Inhomogeneous necrosis of the matrix (circles) close to fibrosclerotic trabeculae (arrows). (E) Bone section with empty lacunae. [Color figure can be viewed at [wileyonlinelibrary.com](https://onlinelibrary.wiley.com)]

increase of empty lacunae per microscopic field were observed in the irradiated bone when compared to nonirradiated bone [19]. Of note, irrespective of the dose, both  $ROI_H$  and  $ROI_L$  showed similar remarkable signs of RT-induced bone damage (Figure 6).

This study has confirmed with radiologic and histologic findings the development of a double irradiation model. On  $ROI_H$ , both histologic and radiologic bone damages were clearly demonstrated in all samples. Thus,  $ROI_H$  can be genuinely defined as ORN model, as it shows similar findings to human ORN. It could be argued that mucosal lesions and other ORN-related clinical manifestations (e.g., pathologic fractures) included in most ORN definitions [5, 10, 29, 30] were absent. However, beside the absence of universally accepted definition criteria for ORN, several studies have proposed to consider an early, uncomplicated phase of ORN as a distinct clinical entity that is diagnosed only through imaging [21, 31, 32]. On the other hand,  $ROI_L$  did not show any radiologic findings of ORN, while the histologic bone alterations paralleled those of  $ROI_H$ . Such findings confirmed that  $ROI_L$  was effectively irradiated, yet with an insufficient dose to generate clinically obvious alterations. Thus,  $ROI_L$  could be arguably defined as an ORN model. The discrepancy between radiologic and histologic findings suggest that  $ROI_L$  could serve as a model of irradiated bone, with normal clinical and radiologic appearance while bearing the biologic injury. To the best of our knowledge, this is the first study proposing a double RT-induced disease model in a single animal [19, 33, 34]. The successful development of an ORN/irradiated bone model reinforces the versatility of New Zealand rabbit in the field of preclinical HN oncology research [35].

The scientific literature offers a few models of mandibular ORN/irradiated bone, which highly differ in terms of animal

host, irradiation schedule and dose, and RT equipment used [28, 33, 34, 36–38]. Among them, rabbit models are convenient compared to mice or rats, as rabbits' dimension and stamina allow adequate clinical evaluation, tolerance to irradiation, and prolonged postirradiation follow-up [39]. Also, in contrast to larger models (e.g., canine model), rabbits are easier to handle and less expensive. A further advantage is the bone turnover rate, which is thrice as fast as the turnover of the human bone, allowing the reduction of follow-up time in rabbits, since an observation period of 6 months could be roughly compared to 2 years in humans [40].

However, studies focused on rabbit models are limited and heterogeneous in terms of dose and irradiation schedule. Eppley et al. [41] and Xu et al. [38, 42] proposed a single-dose irradiation to obtain ORN in rabbits. Despite being time sparing, it substantially deviates from the fractionated regimens used in the human setting. In our study, a fractionated schedule was adopted aiming to more consistently reproduce the current clinical practice. Total dose of irradiation is a well-known risk factor for ORN development [43, 44]. In humans, a total dose of 65–75 Gy increases the risk of ORN, with special reference to its early onset (occurring within 2 years from the end of RT) [45]. In a recent study by Zong et al. [19], a fractionated schedule has been designed through the biological equivalent dose linear quadratic equation, and used to generate an ORN rabbit model. Three different doses were tested (35, 40, and 45 Gy in five fractions) and the dose of 45 Gy in five fractions (9 Gy per fraction) was the minimum dose to obtain mandibular ORN. However, in our study the irradiation dose was reduced to 7 Gy/fraction to partially account for the differences between MV photons, used by Zong et al. [19], and kV irradiations, used in our study.



Of utmost importance, the model we developed demonstrated an excellent safety profile. The desired toxicity induced by RT was obtained, without jeopardizing the model itself. Although a rabbit died during MR acquisition, this event was neither RT-nor ORN-related, resulting in a RT-specific mortality of 0%. The model is simple to realize, easily reproducible, and safe. In addition, it is convenient in terms of costs, since two different clinical conditions (i.e., ORN and irradiated bone) can be modeled in a single animal. We believe it can represent a valid experimental model to be exploited for different aims, including the study of ORN pathogenesis, anti-ORN therapies, and anti-ORN regenerative medicine strategies.

## 5 | Conclusions

The adopted irradiation planning enabled achievement of a double preclinical model in each animal sample, which included both irradiated bone (with normal radiologic appearance and histologic damage) and ORN (with both radiologic and histologic injury).

Feasibility, reproducibility, and the safety profile make this model appealing for basic and translational research in the field of HN oncology.

### Data Availability Statement

The data that support the findings of this study are available from the corresponding author upon reasonable request.

### References

1. G. Delaney, S. Jacob, C. Featherstone, and M. Barton, "The Role of Radiotherapy in Cancer Treatment," *Cancer* 104, no. 6 (2005): 1129–1137, <https://doi.org/10.1002/cncr.21324>.
2. "Guidelines Detail," NCCN, accessed October 30, 2023, <https://www.nccn.org/guidelines/guidelines-detail>.
3. J. A. Langendijk, P. Doornaert, I. M. Verdonck-de Leeuw, C. R. Lee-mans, N. K. Aaronson, and B. J. Slotman, "Impact of Late Treatment-Related Toxicity on Quality of Life Among Patients With Head and Neck Cancer Treated With Radiotherapy," *Journal of Clinical Oncology: Official Journal of the American Society of Clinical Oncology* 26, no. 22 (2008): 3770–3776, <https://doi.org/10.1200/JCO.2007.14.6647>.
4. D. J. Toneatti, R. R. Graf, J. P. Burkhard, and B. Schaller, "Survival of Dental Implants and Occurrence of Osteoradionecrosis in Irradiated Head and Neck Cancer Patients: A Systematic Review and Meta-Analysis," *Clinical Oral Investigations* 25, no. 10 (2021): 5579–5593, <https://doi.org/10.1007/s00784-021-04065-6>.
5. A. Chronopoulos, T. Zarra, M. Ehrenfeld, and S. Otto, "Osteoradionecrosis of the Jaws: Definition, Epidemiology, Staging and Clinical and Radiological Findings. A Concise Review," *International Dental Journal* 68, no. 1 (2018): 22–30, <https://doi.org/10.1111/idj.12318>.
6. H. Y. Sroussi, J. B. Epstein, R. Bensadoun, et al., "Common Oral Complications of Head and Neck Cancer Radiation Therapy: Mucositis, Infections, Saliva Change, Fibrosis, Sensory Dysfunctions, Dental Caries, Periodontal Disease, and Osteoradionecrosis," *Cancer Medicine* 6, no. 12 (2017): 2918–2931, <https://doi.org/10.1002/cam4.1221>.
7. J. J. Thorn, H. S. Hansen, L. Specht, and L. Bastholt, "Osteoradionecrosis of the Jaws: Clinical Characteristics and Relation to the Field of Irradiation," *Journal of Oral and Maxillofacial Surgery* 58, no. 10 (2000): 1088–1093, <https://doi.org/10.1053/joms.2000.9562>.
8. A. J. Frankart, M. J. Frankart, B. Cervenka, A. L. Tang, D. G. Krishnan, and V. Takiar, "Osteoradionecrosis: Exposing the Evidence Not the Bone," *International Journal of Radiation Oncology, Biology, Physics* 109, no. 5 (2021): 1206–1218, <https://doi.org/10.1016/j.ijrobp.2020.12.043>.
9. A. Lyons and N. Ghazali, "Osteoradionecrosis of the Jaws: Current Understanding of Its Pathophysiology and Treatment," *British Journal of Oral & Maxillofacial Surgery* 46, no. 8 (2008): 653–660, <https://doi.org/10.1016/j.bjoms.2008.04.006>.
10. R. E. Marx, "Osteoradionecrosis: A New Concept of Its Pathophysiology," *Journal of Oral and Maxillofacial Surgery* 41, no. 5 (1983): 283–288, [https://doi.org/10.1016/0278-2391\(83\)90294-X](https://doi.org/10.1016/0278-2391(83)90294-X).
11. I. Meyer, "Infectious Diseases of the Jaws," *Journal of Oral Surgery* 28, no. 1 (1970): 17–26.
12. S. Delanian and J. L. Lefaix, "The Radiation-Induced Fibroatrophic Process: Therapeutic Perspective via the Antioxidant Pathway," *Radiotherapy and Oncology: Journal of the European Society for Therapeutic Radiology and Oncology* 73, no. 2 (2004): 119–131, <https://doi.org/10.1016/j.radonc.2004.08.021>.
13. K. T. Fitzgerald, C. Lyons, A. England, et al., "Risk Factors Associated With the Development of Osteoradionecrosis (ORN) in Head and Neck Cancer Patients in Ireland: A 10-Year Retrospective Review," *Radiotherapy and Oncology* 196 (2024): 196, <https://doi.org/10.1016/j.radonc.2024.110286>.
14. M. Renouf, S. Auger, L. Campion, et al., "Prognostic Factors of Mandibular Osteoradionecrosis Including Accurate Colocalization of Avulsions and Dosimetric Dental Mapping Software, a Case-Control Study," *International Journal of Radiation Oncology, Biology, Physics* 120, no. 3 (2024): 783–795, <https://doi.org/10.1016/j.ijrobp.2024.04.019>.
15. L. Merring-Mikkelsen, M. H. Brincker, M. Andersen, Ö. Kesmez, and M. S. Nielsen, "Mandible Osteoradionecrosis After High-Dose Radiation Therapy for Head and Neck Cancers: Risk Factors and Dosimetric Analysis," *Acta Oncologica* 63 (2024): 273–276, <https://doi.org/10.2340/1651-226X.2024.35222>.
16. F. De Felice, V. Tombolini, D. Musio, and A. Polimeni, "Radiation Therapy and Mandibular Osteoradionecrosis: State of the Art," *Current Oncology Reports* 22, no. 9 (2020): 89, <https://doi.org/10.1007/s11912-020-00954-3>.
17. N. Rice, I. Polyzois, K. Ekanayake, O. Omer, and L. F. A. Stassen, "The Management of Osteoradionecrosis of the Jaws—A Review," *Surgeon: Journal of the Royal Colleges of Surgeons of Edinburgh and Ireland* 13, no. 2 (2015): 101–109, <https://doi.org/10.1016/j.surge.2014.07.003>.
18. L. Park, N. Lilic, B. Addison, and R. Patel, "Cost Analysis of Osteoradionecrosis," *Journal of Laryngology and Otology* 131, no. 4 (2017): 303–308, <https://doi.org/10.1017/S0022215116009956>.
19. C. Zong, B. Cai, X. Wen, et al., "The Role of Myofibroblasts in the Development of Osteoradionecrosis in a Newly Established Rabbit Model," *Journal of Cranio-Maxillofacial Surgery* 44, no. 6 (2016): 725–733, <https://doi.org/10.1016/j.jcms.2016.03.002>.
20. M. Bazalova and E. E. Graves, "The Importance of Tissue Segmentation for Dose Calculations for Kilovoltage Radiation Therapy: Tissue Segmentation for Kilovoltage Radiotherapy," *Medical Physics* 38, no. 6 (2011): 3039–3049, <https://doi.org/10.1118/1.3589138>.
21. S. S. Deshpande, M. H. Thakur, K. Dholam, A. Mahajan, S. Arya, and S. Juvekar, "Osteoradionecrosis of the Mandible: Through a radiologist's Eyes," *Clinical Radiology* 70, no. 2 (2015): 197–205, <https://doi.org/10.1016/j.crad.2014.09.012>.
22. G. Granström, "Osseointegration in Irradiated Cancer Patients: An Analysis With Respect to Implant Failures," *Journal of Oral and Maxillofacial Surgery* 63, no. 5 (2005): 579–585, <https://doi.org/10.1016/j.joms.2005.01.008>.

23. J. Bras, H. K. T. De Jonge, and J. P. R. Van Merkesteyn, "Osteoradionecrosis of the Mandible: Pathogenesis," *American Journal of Otolaryngology* 11, no. 4 (1990): 244–250, [https://doi.org/10.1016/0196-0709\(90\)90084-9](https://doi.org/10.1016/0196-0709(90)90084-9).
24. M. Ferrari, S. Taboni, H. H. L. Chan, et al., "Hydrogel-Chitosan and Polylactic Acid-Polycaprolactone Bioengineered Scaffolds for Reconstruction of Mandibular Defects: A Preclinical In Vivo Study With Assessment of Translationally Relevant Aspects," *Frontiers in Bioengineering and Biotechnology* 15, no. 12 (2024): 1353523, <https://doi.org/10.3389/fbioe.2024.1353523>.
25. I. Miyamoto, R. Tanaka, S. Kogi, et al., "Clinical Diagnostic Imaging Study of Osteoradionecrosis of the Jaw: A Retrospective Study," *Journal of Clinical Medicine* 10, no. 20 (2021): 4704, <https://doi.org/10.3390/jcm10204704>.
26. B. Yilmaz, E. Somay, A. Kucuk, B. Pehlivan, U. Selek, and E. Topkan, "Challenges in the Radiological Diagnosis of Osteoradionecrosis of the Jaw in Head and Neck Cancer Patients," in *Advancements in Cancer Research*, ed. C. M. Sergi (Brisbane, AU: Exon Publications, 2023), <https://www.ncbi.nlm.nih.gov/books/NBK594964/>.
27. J. M. Gowgiel, "Experimental Radio-Osteonecrosis of the Jaws," *Journal of Dental Research* 39, no. 1 (1960): 176–197, <https://doi.org/10.1177/00220345600390011401>.
28. L. J. Poort, J. H. B. Ludlage, N. Lie, et al., "The Histological and Histomorphometric Changes in the Mandible After Radiotherapy: An Animal Model," *Journal of Cranio-Maxillofacial Surgery* 45, no. 5 (2017): 716–721, <https://doi.org/10.1016/j.jcms.2017.02.014>.
29. J. A. Chen, C. C. Wang, Y. K. Wong, et al., "Osteoradionecrosis of Mandible Bone in Patients With Oral Cancer—Associated Factors and Treatment Outcomes," *Head & Neck* 38, no. 5 (2016): 762–768, <https://doi.org/10.1002/hed.23949>.
30. J. B. Epstein, F. L. Wong, and P. Stevenson-Moore, "Osteoradionecrosis: Clinical Experience and a Proposal for Classification," *Journal of Oral and Maxillofacial Surgery: Official Journal of the American Association of Oral and Maxillofacial Surgeons* 45, no. 2 (1987): 104–110, [https://doi.org/10.1016/0278-2391\(87\)90399-5](https://doi.org/10.1016/0278-2391(87)90399-5).
31. A. A. Owosho, A. Kadempour, S. K. Yom, et al., "Radiographic Osteoradionecrosis of the Jaw With Intact Mucosa: Proposal of Clinical Guidelines for Early Identification of This Condition," *Oral Oncology* 51, no. 12 (2015): e93–e96, <https://doi.org/10.1016/j.oraloncology.2015.09.009>.
32. G. Støre and M. Boysen, "Mandibular Osteoradionecrosis: Clinical Behaviour and Diagnostic Aspects," *Clinical Otolaryngology and Allied Sciences* 25, no. 5 (2000): 378–384, <https://doi.org/10.1046/j.1365-2273.2000.00367.x>.
33. P. Bléry, F. Espitalier, A. Hays, et al., "Development of Mandibular Osteoradionecrosis in Rats: Importance of Dental Extraction," *Journal of Cranio-Maxillofacial Surgery* 43, no. 9 (2015): 1829–1836, <https://doi.org/10.1016/j.jcms.2015.08.016>.
34. R. S. Jackson, S. G. Voss, Z. C. Wilson, et al., "An Athymic Rat Model for Mandibular Osteoradionecrosis Allowing for Direct Translation of Regenerative Treatments," *Otolaryngology—Head and Neck Surgery: Official Journal of American Academy of Otolaryngology-Head and Neck Surgery* 153, no. 4 (2015): 526–531, <https://doi.org/10.1177/0194599815593278>.
35. N. Muhanna, C. M. Douglas, H. H. L. Chan, et al., "Rabbit VX2 Head and Neck Squamous Cell Models for Translational Head and Neck Therapeutic Technology Development," *Clinical and Translational Medicine* 11, no. 10 (2021): e550, <https://doi.org/10.1002/ctm2.550>.
36. M. Fenner, J. Park, N. Schulz, et al., "Validation of Histologic Changes Induced by External Irradiation in Mandibular Bone. An Experimental Animal Model," *Journal of Cranio-Maxillofacial Surgery* 38, no. 1 (2010): 47–53, <https://doi.org/10.1016/j.jcms.2009.07.011>.
37. G. Wu, L. Chen, T. Qu, G. Zhu, Y. Wang, and C. Zhu, "Ultrasonic Treatment of Canine ORNM," *Journal of Oral and Maxillofacial Surgery* 71, no. 1 (2013): 199–207, <https://doi.org/10.1016/j.joms.2012.03.034>.
38. J. Xu, Z. Zheng, D. Fang, et al., "Early-Stage Pathogenic Sequence of Jaw Osteoradionecrosis In Vivo," *Journal of Dental Research* 91, no. 7 (2012): 702–708, <https://doi.org/10.1177/0022034512448661>.
39. A. Paredes, M. Lindeblad, R. Patil, et al., "The New Zealand White Rabbit Animal Model of Acute Radiation Syndrome: Hematopoietic and Coagulation-Based Parameters by Radiation Dose Following Supportive Care," *International Journal of Radiation Biology* 97, no. 1 (2021): S45–S62, <https://doi.org/10.1080/09553002.2020.1820606>.
40. M. M. Abu-Serriah, D. A. McGowan, K. F. Moos, and J. Bagg, "Extra-Oral Craniofacial Endosseous Implants and Radiotherapy," *International Journal of Oral and Maxillofacial Surgery* 32, no. 6 (2003): 585–592, <https://doi.org/10.1054/ijom.2003.0429>.
41. B. L. Eppley, D. T. Connolly, T. Winkelmann, A. M. Sadove, D. Heuvelman, and J. Feder, "Free Bone Graft Reconstruction of Irradiated Facial Tissue: Experimental Effects of Basic Fibroblast Growth Factor Stimulation," *Plastic and Reconstructive Surgery* 88, no. 1 (1991): 1–11, <https://doi.org/10.1097/00006534-199107000-00001>.
42. J. Xu, Z. Zheng, D. Fang, et al., "Mesenchymal Stromal Cell-Based Treatment of Jaw Osteoradionecrosis in Swine," *Cell Transplantation* 21, no. 8 (2012): 1679–1686, <https://doi.org/10.3727/096368911X637434>.
43. B. R. Chrcanovic, P. Reher, A. A. Sousa, and M. Harris, "Osteoradionecrosis of the Jaws—A Current Overview—Part 1," *Oral and Maxillofacial Surgery* 14, no. 1 (2010): 3–16, <https://doi.org/10.1007/s10006-009-0198-9>.
44. E. Topkan, A. Kucuk, E. Somay, B. Yilmaz, B. Pehlivan, and U. Selek, "Review of Osteoradionecrosis of the Jaw: Radiotherapy Modality, Technique, and Dose as Risk Factors," *Journal of Clinical Medicine* 12, no. 8 (2023): 3025, <https://doi.org/10.3390/jcm12083025>.
45. T. Reuther, T. Schuster, U. Mende, and A. Kübler, "Osteoradionecrosis of the Jaws as a Side Effect of Radiotherapy of Head and Neck Tumour Patients—A Report of a Thirty Year Retrospective Review," *International Journal of Oral and Maxillofacial Surgery* 32, no. 3 (2003): 289–295, <https://doi.org/10.1054/ijom.2002.0332>.

### Supporting Information

Additional supporting information can be found online in the Supporting Information section.